The scorpion planet survey: wide-orbit giant planets around young A-type stars

Wagner, K.; Apai, D.; Kasper, M.; McClure, M.; Robberto, M.

The Astronomical Journal, 163:80 (11pp), 2022 February https://doi.org/10.3847/1538-3881/ac409d

The Scorpion Planet Survey: Wide-orbit Giant Planets Around Young A-type Stars

Kevin Wagner[1,2,3], Dániel Apai[1,2,4], Markus Kasper[5], Melissa McClure[6], and Massimo Robberto[7]
[1] Steward Observatory, University of Arizona, USA; kevinwagner@email.arizona.edu
[2] NASA NExSS Alien Earths Team, USA
[3] NASA Hubble Fellowship Program—Sagan Fellow, USA
[4] Lunar and Planetary Laboratory, University of Arizona, USA
[5] European Southern Observatory, Germany
[6] University of Leiden, Netherlands
[7] Space Telescope Science Institute, USA
Received 2021 August 13; revised 2021 November 26; accepted 2021 December 3; published 2022 January 21

Abstract

The first directly imaged exoplanets indicated that wide-orbit giant planets could be more common around A-type stars. However, the relatively small number of nearby A-stars has limited the precision of exoplanet demographics studies to $\gtrsim$10%. We aim to constrain the frequency of wide-orbit giant planets around A-stars using the VLT/SPHERE extreme adaptive optics system, which enables targeting $\gtrsim$100 A-stars between 100 and 200 pc. We present the results of a survey of 84 A-stars within the nearby ∼5–17 Myr old Sco OB2 association. The survey detected three companions—one of which is a new discovery (HIP 75056Ab), whereas the other two (HD 95086b and HIP 65426b) are now-known planets that were included without a priori knowledge of their existence. We assessed the image sensitivity and observational biases with injection and recovery tests combined with Monte Carlo simulations to place constraints on the underlying demographics. We measure a decreasing frequency of giant planets with increasing separation, with measured values falling between 10% and 2% for separations of 30–100 au, and 95% confidence-level upper limits of $\lesssim$45%–8% for planets on 30–100 au orbits, and $\lesssim$5% between 200 and 500 au. These values are in excellent agreement with recent surveys of A-stars in the solar neighborhood−supporting findings that giant planets out to separations of $\lesssim$100 au are more frequent around A-stars than around solar-type hosts. Finally, the relatively low occurrence rate of super-Jupiters on wide orbits, the positive correlation with stellar mass, and the inverse correlation with orbital separation are consistent with core accretion being their dominant formation mechanism.

Unified Astronomy Thesaurus concepts: Exoplanets (498); Exoplanet formation (492); Exoplanet systems (484); Early-type stars (430); Direct imaging (387); Coronagraphic imaging (313)

1. Introduction

High-contrast imaging enables studying wide-orbit giant planets around young stars. However, the number of directly imaged planets remains low (on the order of tens). After hundreds of nearby Sun-like (FGK) stars were observed over multiple surveys reporting null detections (e.g., Chauvin et al. 2003; Biller et al. 2007; Kasper et al. 2007; Apai et al. 2008; Nielsen et al. 2013), the first exoplanets discovered by direct imaging−including the four super-Jovian planets orbiting the A5V star HR 8799 (Marois et al. 2008, 2010) and the giant planet orbiting the A6V star β Pictoris (Lagrange et al. 2010)—seemed to indicate that giant planets on orbits of ∼10 au or greater are more common around higher-mass stars.

If the cores of wide-separation giant planets are typically assembled via the slow, step-wise process of core accretion (e.g., Pollack et al. 1996), which strongly depends on the local surface density of solids and orbital timescales in protoplanetary disks (and hence on stellar mass: e.g., Pascucci et al. 2016), then wide-orbit giant planets should be more frequent around higher-mass stars. This is indeed true for close-in giant planets (e.g., Ghezzi et al. 2018), and this trend should extend to larger radii if the majority of wide-orbit giant planets form similarly via core accretion. The systems mentioned above were followed up by discoveries of several other planets around A-type stars −including those orbiting HD 95086 (Rameau et al. 2013), HD 106906b (Bailey et al. 2014), 51 Eri (Macintosh et al. 2015), and HIP65426 (Chauvin et al. 2017). It is also worth noting that an increasing number of planets have been imaged around lower-mass stars—including the two planets orbiting the K7 (0.76 $M_{\odot}$) star PDS 70 (Keppler et al. 2018; Wagner et al. 2018; Haffert et al. 2019) and three planets around K-stars from the Young Suns Exoplanet Survey (YSES; Bohn et al. 2020, 2021). While the number of imaged planets around FGK stars has increased in recent years, there remain fewer than those around A-type stars. Considering even lower-mass (M-dwarf) stellar hosts, Lannier et al. (2016) also find a lower occurrence rate of wide-orbit giant planets compared to those around A-stars.

The recent Gemini Planet Imager Exoplanet Survey (GPIES; Nielsen et al. 2019) presented interim results that indicate a significant (>99% confidence-level; CL) difference between the wide-orbit giant planet populations of high-mass and low-mass stars. For planets between 5 and 13 $M_{\rm Jup}$, and between $a = 10$–100 au orbiting >1.5 $M_{\odot}$ stars, they found a 68%-CL interval of 5.3%–13.9%; whereas similar planets orbiting stars of any spectral type yielded a 68%-CL interval of 2.1%–5.4%. Similarly, the SHINE survey on VLT/SPHERE (Vigan et al. 2021) that includes many of the same targets yielded a 68%-CL interval of 13.3%–36.5% for the frequency of 1–75 $M_{\rm Jup}$, and between $a = 5$–300 au orbiting B/A-type stars[8] and 3.0%–

[8] Note that the larger value is reflective of the larger range of parameters, particularly at lower masses and semimajor axes for which planets are more frequent.

10.5% for planets of similar properties orbiting FGK stars. Both samples included >50 BA-type stars (>70 for GPIES) among the nearby moving groups.

The metaanalysis of directly imaged planets and brown dwarf companions by Wagner et al. (2019) including all known systems with detected companions also found a steeper relative companion mass function for high-mass stellar hosts compared to low-mass stellar hosts. However, the trend may not extend to all separations. Considering companions on wider orbits of 30–300 au, Bowler (2016) found no significant difference between giant planet populations around high-mass stars and low-mass stars ($2.8^{+3.7}_{-2.3}$% of BA stars, <4.1% of FGK stars, and <3.9% of M dwarfs). Nevertheless, at separations of $\lesssim$100 au, the message appears clear: higher-mass stars have a higher frequency of hosting giant planets.

The higher frequency of wide-orbit giant planets around A-stars influences models of planet formation and the target lists (and expected yields) of future surveys. However, the occurrence rate of wide-orbit giant planets around high-mass stars remains significantly uncertain. Upper limits range from $\lesssim$20% (GPIES: 95%-CL, 5–13 $M_{\rm Jup}$, 10–100 au; Nielsen et al. 2019) to $\lesssim$36.5% (SHINE: 68%-CL, 1–75 $M_{\rm Jup}$, 5–300 au; Vigan et al. 2021). These state-of-the-art surveys utilize the latest in extreme adaptive optics (ExAO) technology. However, they were also designed (with good reason) to maximize discoveries of planets on shorter periods by focusing on nearby stars. This limits the available number of A-stars, and particularly those with well-constrained ages. Well-constrained ages translate to better constraints on planetary masses (and upper limits) because planetary luminosity is correlated with both mass and age.

An opportunity to better constrain the demographics of wide-orbit giant planets around A-type stars has recently arisen with the advent of ExAO systems on large ground-based telescopes (e.g., Macintosh et al. 2014; Jovanovic et al. 2015; Males et al. 2018; Beuzit et al. 2019). These systems routinely reach contrasts of $\sim 10^{-6}$ for stars within young moving groups at distances of $\gtrsim$100 pc, which enables homogeneous surveys of a large number of A-stars with well-constrained ages. The Sco OB2 association (also known as Scorpius–Centaurus–Lupus; Sco-Cen) at ~100–200 pc contains the largest number of nearby age-dated A-stars (de Zeeuw et al. 1999; Kouwenhoven et al. 2005, 2007). The ages of the stars within Sco OB2 vary between ~5 and 17 Myr, depending on position within the cluster (Pecaut & Mamajek 2016). At such young ages, the population of recently formed giant planets is luminous enough to be imaged down to ~4–5 $M_{\rm Jup}$ at separations $\gtrsim$30 au (e.g., Fortney et al. 2008; Baraffe et al. 2015; Marleau et al. 2019).

The goal of this survey is to directly constrain the demographics of wide-orbit giant planets around the A-stars of the Sco OB2 association in order to inform planet-formation models (e.g., Forgan et al. 2018; Emsenhuber et al. 2021), the target selections and expected yields of future surveys, and other areas where this fundamental parameter is relevant. We also aim to discover additional planets and substellar companions whose orbits and atmospheres are accessible to direct characterization. Finally, the results of this survey will be directly comparable to the demographics of planets around A-stars in the closer (but slightly older) moving groups targeted largely by past surveys (e.g., Nielsen et al. 2019; Vigan et al. 2021), and also to lower-mass members of the Sco OB2 association (Bohn et al. 2020, 2021)—enabling trends in exoplanet properties to be identified across host star age, mass, and formation environment.

2. Observations and Data Reduction

Our observations utilized the Spectro-Polarimetric High-Contrast Exoplanet Research Experiment (SPHERE) instrument on the Very Large Telescope (VLT) in Chile (Beuzit et al. 2019). SPHERE provides contrasts of $10^{-5} - 10^{-6}$ at separations of ~1″ in under an hour for ~7–8 mag stars. SPHERE also provides diffraction-limited imaging with a resolution of ~0.″05 across wavelengths of ~1–2.2 μm. Dual-band imaging in a selection of narrow-band filters over a field of view of ~6″ in radius (IRDIS; Vigan et al. 2010) is combined with simultaneous integral field spectroscopy from 0.95–1.65 μm over a smaller field of view of 0.″8 in radius (IFS; Claudi et al. 2008). The latter enables spectral identification of close-in exoplanet candidates, while the dual-band imaging enables identifying companions on wider orbits through their common proper motion.

Our observations typically utilized the IRDIFS_Ext mode of SPHERE, in which dual-band images are acquired with IRDIS in the K12 filters ($\lambda_{\rm K1} = 2.110 \pm 0.051$ μm, $\lambda_{\rm H2} = 2.251 \pm 0.055$ μm) and spatially-resolved spectra from $Y-H$ band (0.95–1.65 μm, $R \sim 30$) are acquired with the IFS. For some of the targets (primarily among the systems that were observed by SPHERE for other programs) the IRDIFS mode was used. This includes the $H23$ dual-band filter combination ($\lambda_{\rm H2} = 1.593 \pm 0.026$ μm, $\lambda_{\rm H3} = 1.667 \pm 0.027$ μm) and IFS spectroscopy from $Y-J$ (0.95–1.35 μm, $R \sim 50$). Each target was observed for approximately ~30–60 minutes of exposure time (see Appendix), enabling field rotation of ~20–30°, and resulting in similar performance for each target.

2.1. Target Selection

Targets were selected from the A-stars within the Sco OB2 association, which contains the largest group of nearby A-stars with well-determined ages (de Zeeuw et al. 1999). Typical ages and distances to member systems range from ~10 to 17 Myr and ~100 to 200 pc (Pecaut & Mamajek 2016; Gaia Collaboration et al. 2018). The list of A-stars among this association is thought to be complete. However, A-stars have a high (~50%) binary fraction, which limits the available orbital phase space. Kouwenhoven et al. (2005) and Kouwenhoven et al. (2007) performed an early AO survey of these systems using the ADONIS system on the 3.6 m New Technology Telescope. This survey established which A-stars host stellar companions at projected separations of $\gtrsim$0.″2.

From the list of 115 A-star systems in Kouwenhoven et al. (2005, 2007), we selected those that may be capable of hosting wide-orbit planetary systems. The gravitational influence of a companion star will restrict the range of stable planetary orbits to those that are $\lesssim$25%–30% of the stellar companion's periapsis (Holman & Wiegert 1999). For distances of ~100 pc, a planet on a stable ~50 au orbit translates to a minimum binary separation of $\gtrsim$1.″5. We removed those with smaller projected separations from the list, which resulted in 97 systems. Among these, we observed 63 throughout 2015–2019, and obtained publicly available data sets from the European Southern Observatory (ESO) archive for another 25 systems. This resulted in a total survey size of 88 Sco-Cen A-stars (see Table A1). Of these observations, four were deemed of inferior

quality, typically due to very low field rotation ($\lesssim 5°$), and were excluded from the analysis. These include targets with Survey-ID S26, S57, S58, and SA29.

2.2. Automated Data Reduction Pipeline

We reduced the data for each target in a uniform manner with a self-developed automated pipeline designed to take raw data products from the ESO archive and to assemble the high-level scientific products.[9] For single stars, this pipeline works well with no intervention. However, some intervention is needed in the case of wide binary systems (i.e., to mask the companion) or observations taken with a nonstandard approach (e.g., those lacking standard calibrations). The pipeline results in point-spread function (PSF) subtracted images, signal-to-noise ratio (S/N) maps generated according to Mawet et al. (2014), contrast curves generated through synthetic planet injections (with a S/N threshold set to 5), and lists of candidate sources above a given S/N threshold (set to 3.5 for initial identification and vetting).

The data reduction pipeline began with the procedures presented in Apai et al. (2016) and was improved sequentially throughout the survey (Wagner et al. 2015, 2016, 2018, 2020). The pipeline is briefly summarized here. Basic calibrations, including dark subtraction, flat field division, and determination of the coronagraphic centering via satellite spots (typically taken at the start of the observation), were performed for all data sets. For relevant epochs (those prior to 2016 July), the time synchronization correction of Maire et al. (2016) was applied to the parallactic angle information, and for all epochs the Maire et al. (2016) astrometric and field distortion corrections were applied. For single-star targets, the images were then aligned in the pupil-stabilized orientation via cross correlation. For multistar systems, or those with bright background contaminants, the cross correlation was either performed on only a central image patch (for widely separated companions) or in the field-stabilized orientation for more closely separated binaries in which the wings of the PSF interfere with alignment.

At this stage (when relevant) synthetic point sources were injected into the data using unsaturated frames taken through a neutral density filter with the target slewed $\sim 0\farcs5$ off of the coronagraph. The PSF was then subtracted via two independent means: via classical angular differential imaging (Marois et al. 2006) and via projection onto eigen images via the Karhunen–Loève image-processing algorithm (Soummer et al. 2012). Given the difference in sensitivity to typical exoplanet spectral features between the K1 and K2 (H2 and H3) images, the K1 (H2) images were utilized for the subsequent analysis, except where color-based information is relevant (i.e., vetting of initial candidates).

2.2.1. Candidate Identification and Follow-up Strategy

Candidates were identified both visually and via an automated S/N-based approach. For each pixel, we measure the flux in an aperture of diameter equivalent to the full width at half maximum, and noise in nonoverlapping apertures at the same radius. We exclude immediately adjacent apertures to minimize the impact of negative side-lobes of true signals introduced by the ADI-based PSF subtraction. We then utilize Equation (9) of Mawet et al. (2014) to calculate the S/N. Systems with candidates of $S/N \geqslant 3.5$ were included in subsequent follow-up imaging. Many systems are near the galactic plane and hence the background contamination fraction is relatively high ($\gtrsim 50\%$ of the targets have at least one background object within the field of view). Ultimately, we attempted to follow-up all observations with plausible exoplanet candidates and were able to re-observe 35 out of 40 systems with identified candidates. One candidate was verified as comoving (HIP 75056Ab, Wagner et al. 2020), and two were identified as known planetary companions (HD 96085b and HIP 65426b; Rameau et al. 2013 and Chauvin et al. 2017). These are shown in Figure 1 and described in Table 1. The rest were identified as background objects by their relative proper motion.

For the five systems (S54, SA6, SA10, SA11, and SA25) with detected sources that were not reobserved (mostly within crowded fields and at separations greater than several arcsec), we consider these sources as likely background stars and adjusted the detection limits according to the brightest ambiguous source. A more sophisticated treatment of the systems that were not followed up would incorporate additional parameters for the possibility that the detected sources may be bound. However, given the nature of these sources and the fact that they lie in a region of parameter space that other studies have probed with greater sensitivity, these prior probabilities are close to zero. We also checked that removing these systems from analysis completely does not significantly alter the results.

2.3. Sensitivity Analysis

We assessed the sensitivity of the data through simulated companion injection and retrieval tests. After image alignment (but prior to high-pass filtering and PSF subtraction) we injected scaled versions of the mean of the off-axis flux calibration frames[10] and proceeded with the following steps of the data reduction. We blocked regions contaminated by bright binary companions or background stars with NaN values, and measured the S/N at the position of injection according to Mawet et al. (2014). We iterated upon the brightness of the source until it was recovered within 5% of S/N = 5. We repeated the process at separations from $0\farcs1$ to $5''$ and at 10 evenly distributed azimuthal angles (beginning with PA = 0°), and then took the median of the sensitivity over azimuth. The results are shown in Figure 2.

For K1 data sets, we reach a median background-limited (5σ) contrast of $\sim 3 \times 10^{-6}$ at separations of $\gtrsim 1\farcs5$. For $H2$ data sets, we reach a similar median background-limited contrast of $\sim 10^{-6}$. These detection limits correspond to masses of ~ 4 and $\sim 2\,M_{\rm Jup}$ (Baraffe et al. 2003) for an age of 15 Myr and distance of 125 pc around a $K = 6$ ($H = 6.5$) star.[11] In the best cases, we reach contrasts $\sim 3\times$ lower than the median background limits, enabling planets as low as $\sim 1\,M_{\rm Jup}$ to be identified around a handful of targets. In the worst cases, the S/N = 5 background limits are ~ 2–3×10^{-5} for some of the K1 data sets, which corresponds to masses of $\sim 6\,M_{\rm Jup}$. At $\sim 0\farcs5$, we reach median-contrasts of $\sim 10^{-5}$ in both K1 and $H2$, which corresponds to

[9] Our open source pipeline is publicly available at https://github.com/astrowagner/sphere-tools/releases/tag/v1.2.

[10] Taken with a neutral density filter (typically ND1.0 or ND2.0, which transmit ~10% and ~1%, respectively). See https://www.eso.org/sci/facilities/paranal/instruments/sphere/inst/filters.html for more details.

[11] The poorer background-limited sensitivity for K1 data sets is due to the higher sky background at longer wavelengths.

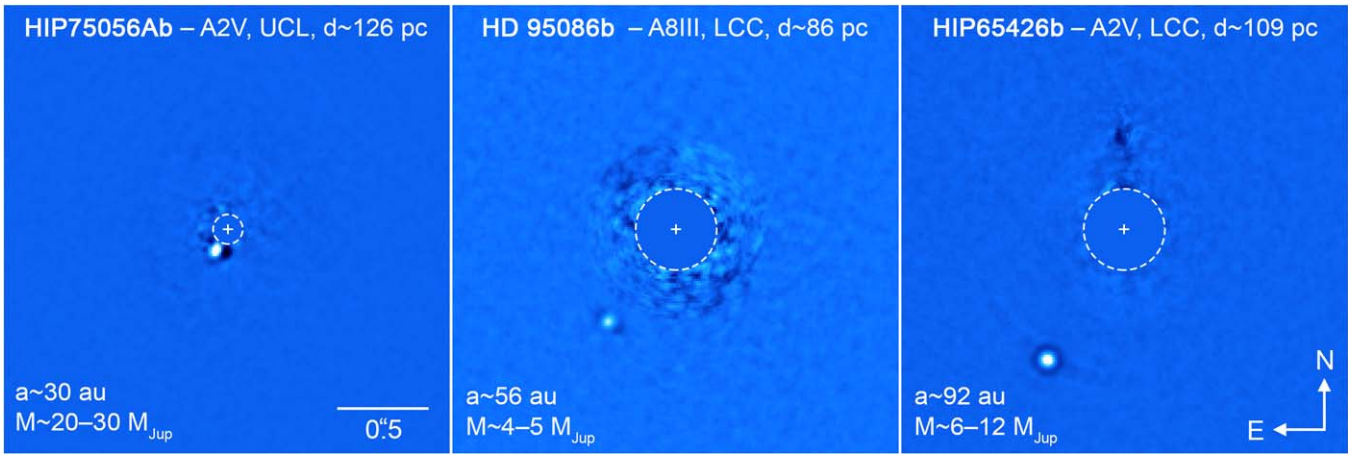

Figure 1. Confirmed substellar companions among Sco-Cen A-type stars. These three objects span masses of ∼4–30 $M_{\rm Jup}$ and separations of ∼15–100 au. The discoveries and initial analyses of HIP 75056Ab, HD 95086b, and HIP 65426b can be found in Wagner et al. (2020), Rameau et al. (2013), and Chauvin et al. (2017), respectively.

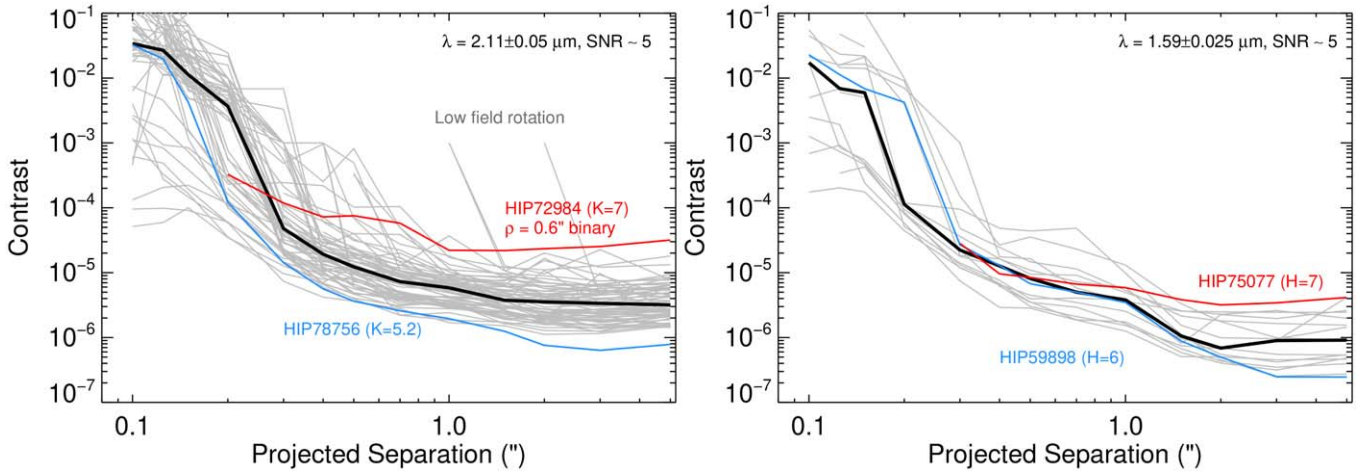

Figure 2. Left: sensitivity of the Scorpion Planet Survey in the K1 band for IRDIFS_Ext observations. Right: sensitivity in H2-band for IRDIFS observations. In both panels the thick black curve shows the median sensitivity, while the blue and red curves show the best and worst cases for background-limited sensitivity.

Table 1
Substellar Companions Imaged around Sco-Cen A-type Stars in This Survey

Name	Sub group	Age (Myr)	Proj. Sep.	Mass ($M_{\rm Jup}$)	a	e	i	Dist.[a] (pc)	Host SpT	SpT	References
HIP 75056Ab	UCL	∼12	0.″15	25 ± 5	30 ± 15 au	0.5 ± 0.2	23 ± 11°	126 ± 2	A2V	M6−L2	b
HD 95086b	LCC	17 ± 4	0.″6	4–5	59^{+10}_{-13}	$0.14^{+0.07}_{-0.14}$	$150^{+12\circ}_{-13}$	86.4 ± 0.4	A8V	L1−T3	c, d, e
HIP 65426b	LCC	14 ± 4	0.″8	6–12	94^{+28}_{-45}	$0.55^{+0.42}_{-0.22}$	$112^{+14\circ}_{-18}$	109.2 ± 0.8	A2V	L5−L7	e, f

Note. [a] Gaia Collaboration et al. (2018), [b] Wagner et al. (2020), [c] Rameau et al. (2013), [d] De Rosa et al. (2016), [e] Bowler et al. (2020), [f] Chauvin et al. (2017).

∼5 $M_{\rm Jup}$. Notably, we find a relatively uniform sensitivity to $\gtrsim$5 $M_{\rm Jup}$ planets at projected separations of $\gtrsim$50 au.

2.4. Monte Carlo Modeling

Previous studies have focused on exploring the scaling relations of planet frequency with physical parameters such as semimajor axis and mass through Markov chain Monte Carlo simulations. Typically, power laws in mass and semimajor axis distributions (and sometimes additional parameters, such as stellar mass; Nielsen et al. 2019) are explored in conjunction with frequency. Since each power law is unknown, as well as the frequency, these three parameters are degenerate with one another. Here, we do not try to replicate this approach, and instead seek to constrain only the frequency of planets (in defined mass and semimajor axis bins) while remaining agnostic to the underlying scaling relations. For this, we utilize a simpler Monte Carlo (MC) simulation of our survey to translate the measured sensitivity to constraints on the underlying planet population (following the approach of Kasper et al. 2007).

We assumed a normally distributed prior on host star distance, with distances obtained from parallaxes reported by Gaia Collaboration et al. (2018). We assumed ages of 10 Myr, which is near the average age of the association

(Pecaut & Mamajek 2016). Since our sample was drawn with representation from the different subgroups, the spread of ages among our sample is representative of the spread of ages among the Sco OB2 association (∼5–17 Myr), which effectively incorporates the uncertainty in age. We assumed uniform prior mass and semimajor axis distributions to generate a large number of companions spanning the available parameter space. Note that the MC serves only to simulate a large number of planets to be compared to the detection limits, and the chosen prior distributions here do not significantly impact our results (we verified that this is the case by also testing assumed distributions of $f \propto M^{-0.5}$, $M^{-1.0}$, and $M^{-1.5}$).

This approach is applicable at this step since we are only concerned with the ratio of detected versus non-detected planets in relatively small predetermined bins (compared to the range over which we later report the frequency). These bins are also defined in a manner such that the sensitivity across each bin is nearly uniform. We randomly generated planets on circular orbits with a uniform prior in the cosine of inclination (see the Appendix of Brandt et al. 2014 and references therein for a discussion of the effects of nonzero eccentricity, which are of secondary importance). In this manner, 4000 companions were simulated for each star with masses between $M = 0.1$–$35\,M_{\rm Jup}$ and $a = 2$–550 au. This generated a sufficient level of smoothness within the individual maps—i.e., runs with greater numbers of simulated companions do not alter or improve the results.

We utilized the models of Baraffe et al. (1998, 2003, 2015) to convert mass to estimated luminosity. The choice of these high-entropy models is motivated by recent work (e.g., Marleau et al. 2019) indicating that the low-entropy models (e.g., Marley et al. 2007; Fortney et al. 2008), in which a large portion of the accretion-generated heat escapes during formation, are an unlikely outcome of giant planet formation. We calculated the ratio of detected versus non-detected companions over a predetermined grid of mass and semimajor axis bins[12] to estimate the completeness to planets around each star. These individual completeness maps were summed to create a total estimated completeness map for the survey—shown in the left panel of Figure 3. In other words, this map shows the number of stars around which we would expect to have observed planets of a given mass and semimajor axis if they were uniformly present.

2.5. Statistical Methods

Two-dimensional Gaussian profiles were constructed for each companion based on their available constraints on mass and semimajor axis. These were normalized such that the sum over each is equal to unity to represent a single detected companion. These were then summed to create a detection probability map to be compared to the completeness map (Figure 3, left). We consider only masses above $\sim 5\,M_{\rm Jup}$ and separations of $a \geqslant 30$ au in order to restrict the analysis to the region in which the sensitivity is relatively uniform. We then explored the consistency of the detections across several ranges of semimajor axes[13] with the average expected number of stars around which we would have been capable of detecting such planets within the set range.

We calculated confidence intervals via the binomial distribution, which gives the probability of a number of successful events occurring among a certain number of trials with a given underlying frequency. For this, we rounded the number of detected companions and average completeness to the nearest integer. For each bin, we report the measured detection rate, along with the frequencies that are consistent with the data at both the 68%-CL and 95%-CL. For bins in which the number of detected companions rounds to zero (i.e., those at >120 au), we report only 95%-CL upper limits (Figure 3).

3. Results

3.1. Detected Companions

While the main result of our survey is its statistical analysis, the number of detected companions is small enough to briefly consider their properties on an individual basis. The detected companions are described in Table 1 and shown in Figure 1. They span masses of several times that of Jupiter to $\sim 25\,M_{\rm Jup}$ and projected separations of ∼15–90 au. Their established properties and relevant references are summarized briefly below.

3.1.1. HIP 75056Ab

HIP 75056Ab is the most massive substellar companion among the sample and that of the shortest orbital period. This ~ 20–$30\,M_{\rm Jup}$ companion at $\sim 0\farcs15$ to an A2V star was discovered as part of our survey (Wagner et al. 2020). It orbits the primary component of a wide-separation ($5\farcs2$) binary with a mass ratio of $q \sim 0.16$ within the Upper Centaurus Lupus (UCL) subgroup of Sco OB2. HIP 75056Ab was detected in 2015 and 2019—establishing that it is comoving with the system on an orbit of $a = 30 \pm 15$ au and $e = 0.5 \pm 0.2$. From IFS data combined with the companion's K1 and $K2$ photometry, Wagner et al. (2020) inferred a spectral type of M8 ± 1 and a temperature of 2300 ± 300 K. From our sensitivity and completeness analysis, we estimate that we would be sensitive to ∼3 such companions if they had an occurrence rate of one per star. The detection of this companion in a region of parameter space with such relatively low sensitivity is likely indicative of a relatively high frequency of companions at smaller separations, and not a higher relative frequency of more massive companions due to the sharply decreasing frequency of companions more massive than ~ 10–$20\,M_{\rm Jup}$ at all separations (e.g., Wagner et al. 2019).

3.1.2. HD 95086b

HD 95086b is the least-massive companion detected in our survey. This ~ 4–$5\,M_{\rm Jup}$ exoplanet was discovered by Rameau et al. (2013) with VLT/NaCo. The host is a single A8 pre-main-sequence star toward the near side of the Lower Centaurus Crux (LCC) subgroup of the Sco OB2 association. The planet is on an orbit with $a \sim 40$–70 au and $e \lesssim 0.2$ (Bowler et al. 2020). The system also hosts a debris disk (Su et al. 2017) with a background galaxy in projected separation (Zapata et al. 2018). From our sensitivity and completeness analysis, we estimate that we would have the capability to detect such a companion around ∼7 stars.

[12] The grid was defined as a = [1, 5, 10, 15, 20, 30, 40, 50, 60, 70, 80, 90, 100, 120, 150, 200, 300, 400, 500] au × M = [0.1, 0.5, 1, 2, 3, 4, 5, 6, 7, 8, 9, 10, 11, 12, 13, 14, 15, 20, 25, 30, 35] $M_{\rm Jup}$. The widths of the bins were set to 10% of the values at each grid point.

[13] Specifically, we assesed the frequency of giant planets of $M = 5$–$35\,M_{\rm Jup}$ in semimajor axis bins of 30–40 au, 40–60 au, 60–80 au, 80–120 au, 120–200 au, 200–300 au, and 300–450 au. These correspond to regions with near-uniform sensitivity.

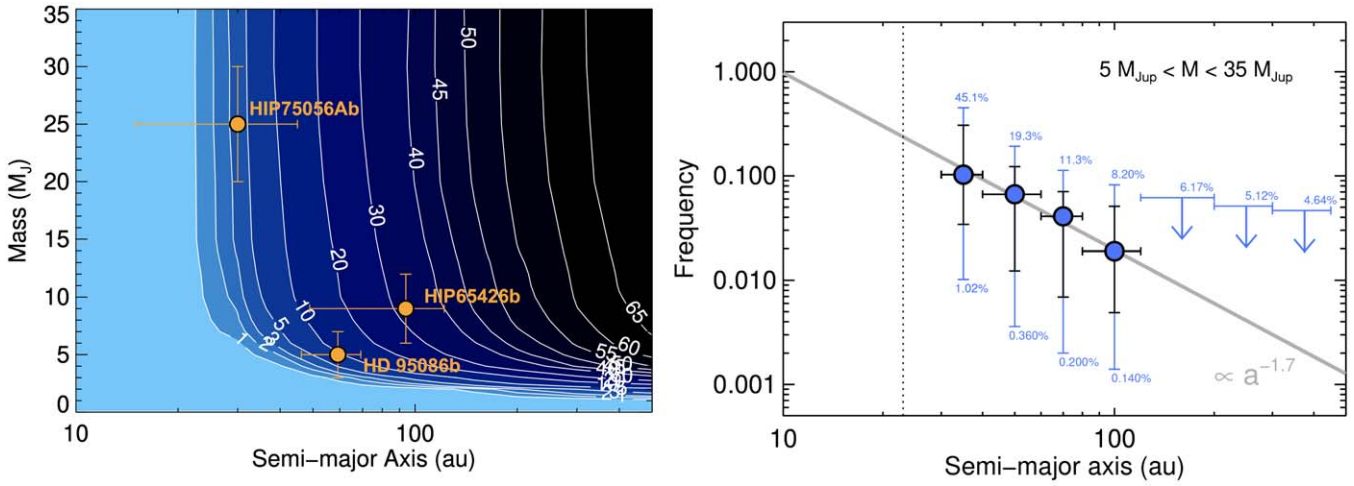

Figure 3. Left: sensitivity of the Scorpion Planet Survey from Monte Carlo simulations. The contours identify the number of stars around which a planet of a given mass and semimajor axis would have resulted in a detection if they were uniformly present. Right: frequency vs. semimajor axis. The blue points show the measured frequency, whereas the vertical (black) uncertainty shows the 68% confidence interval. The blue ranges denote upper and lower 95% confidence values (i.e., their range denotes the 90% confidence interval). The horizontal bars represent the range of the semimajor axis bins. A power law of $f \propto a^{-1.7}$ is shown for comparison (i.e., not as a best fit). The vertical dotted line denotes the inner-most region (∼23 au) at which we would expect to have found ⩾1 companion if they were uniformly present.

3.1.3. HIP 65426b

At a projected separation of ∼90 au, HIP 65426b is the widest-separation companion detected in our survey. This ∼6–12 M_{Jup} companion was discovered by Chauvin et al. (2017) as part of the SHINE survey (Vigan et al. 2021). This companion is the most similar in properties among those detected here to the iconic HR 8799b (Marois et al. 2008), which is the type of companion whose frequency our survey was designed to constrain ($M \sim 5\,M_{Jup}$, $a \sim 70$ au). From our sensitivity analysis, we estimate that we would have the capability to detect a companion such as HIP 65426b around ∼27 stars. A trend that small-separation companions (between ∼5 and 30 M_{Jup}) are more frequent may already be apparent.

3.2. Wide-orbit Giant Planet Frequency

This survey was designed primarily to constrain the frequency of wide-orbit super-Jupiters, with HR 8799-b at ∼70 au as the prime example (Marois et al. 2008, 2010). In other words, we are primarily focused on those between $M = 5$–$15\,M_{Jup}$ and $a = 60$–80 au. Within this range, we measured a frequency of $3.4^{+5.4}_{-2.5}$% and establish a 95%-CL upper limit of ⩽13.9%. This is somewhat lower than (but consistent with) values from other recent surveys, for reasons that will be discussed in Section 4. We also explored frequency constraints at different separations and across a broader range of masses (5–35 M_{Jup}). The measurements of giant planet frequency versus semimajor axis are shown in the right panel of Figure 3. For companions with $M = 5$–$35\,M_{Jup}$ and $a \sim 30$–40 au (80–120 au), we measured observed frequencies of ∼10% (∼2%), with a 95% upper limit of ⩽45% (⩽8%). Consistent with the results of most other surveys, we measure a decreasing frequency of companions with semimajor axis.

3.3. Protoplanetary and Debris Disks

While our observations were designed to directly image exoplanets, they are also sensitive to scattered light from circumstellar dust. Here, we briefly and qualitatively describe those results. We obtained the first images of the debris disk around HD 110058 (Kasper et al. 2015) and the spiral protoplanetary disk around HD 100453 (Wagner et al. 2015), which were both inferred to exist through their infrared spectral energy distributions (SEDs).[14] The presence of such disks (especially the relatively massive disk round HD 100453) is evidence of the youth of Sco OB2, which is in line with recent estimates of the maximum age of ⩽17 Myr (Pecaut & Mamajek 2016). While these disks lower the sensitivity to planets within these systems (accounted for via synthetic injections), they also open additional opportunities for planet formation research (e.g., Dong et al. 2016; Wagner et al. 2018; Nealon et al. 2020), through, for instance, studying disk structures as tracers of dynamical processes.

3.4. HD 131399Ab

In Wagner et al. (2016), we reported the detection of a planetary-mass companion on an ∼80 au orbit within the HD 131399 quadruple system (at the time thought to be a triple; Lagrange et al. 2017). Subsequent observations determined that this object is likely to be a high-velocity background star with its own significant proper motion aligned with the system (Nielsen et al. 2017). Here, we report additional observations in support of this hypothesis. Our extended time baseline covers several years and displays a clear parallax difference between this object and the HD 131399 system that is most notably seen in the plot of position angle versus time (Figure 4). This confirms that it is indeed a background object. HD 131399 and its planet-hosting classification history carry a useful lesson, as assumptions of a stationary background are still commonly assumed. The background object has an approximate proper motion of -5 mas yr^{-1} and -11 mas yr^{-1} in R.A. and decl., respectively, and an parallax of ⩽1 mas (i.e., a distance of ⩾1 kpc and a 2D relative velocity of ⩾57 km s^{-1} with respect to the Sun). This motion is aligned with the system such that initial common proper motion tests yielded an incorrect classification of the object as a likely bound companion.

[14] However, we did not detect several other disks among our sample that were also identified through their SEDs.

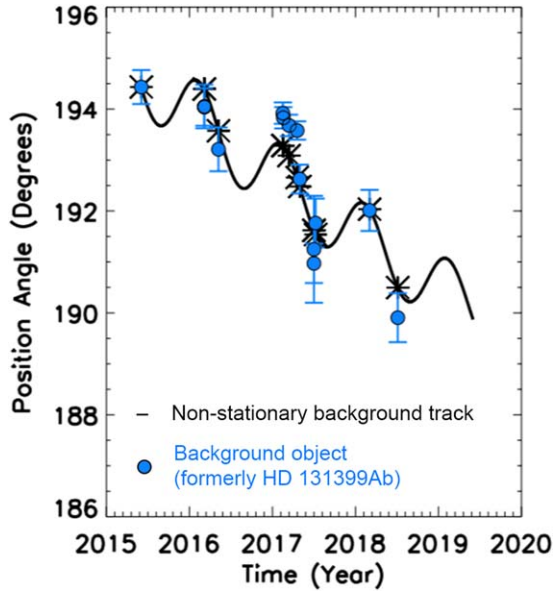

Figure 4. Evolution of relative position angle vs. time of the background object near HD 131399A. The response to the foreground system's (HD 131399's) greater parallax is most notably apparent in the 2017 and 2018 yr, which confirms this previous exoplanet candidate as a background contaminant.

4. Discussion

The primary scientific motivation of this survey is to constrain the frequency of wide-orbit super-Jovian planets orbiting A-stars. Few planet formation models, if any, predict a significant ($\gtrsim$10%) occurrence rate of $\sim$5–15 $M_{\rm Jup}$ planets at $\sim$70 au around hosts of any stellar type. Therefore, this parameter is a fundamental test of the existing models (e.g., Pollack et al. 1996; Boss 1997; Mordasini et al. 2009, 2012; Forgan et al. 2018; Emsenhuber et al. 2021, etc.) and one that is becoming better constrained as the instrumentation progresses.

The frequency of wide-orbit giant planets around A-type stars is also relevant to determine the future yield of exoplanet imaging surveys. For this, trends with separation play a crucial role, as more parameter space is becoming accessible at smaller separations as AO technology improves along with increasing primary mirror diameters. The evidence so far suggests quite strongly that giant planet occurrence rates increase toward smaller separations (until a few au; Fernandes et al. 2019; Fulton et al. 2021). However, the frequency of such companions remains largely uncertain. This is often the reason why surveys report occurrence rates over a wide range of parameters. In order to utilize a survey's best sensitivity, constraints must necessarily come from the outer regions ($\gtrsim$30 au). Often, ranges for reported frequencies extend over hundreds of au, and are easily misinterpreted as implying greater precision than actually exists for planets at the smaller ends of the semimajor axis and mass ranges.

Recently, Nielsen et al. (2019) and Vigan et al. (2021) reported frequencies for giant planets orbiting BA stars of 9^{+5}_{-4}% (M = 5–13 $M_{\rm Jup}$, a = 10–100 au), and $23.0^{+13.5}_{-9.7}$% (M = 1–75 $M_{\rm Jup}$, a = 5–300 au), respectively. Over the same range as Nielsen et al. (2019), we measure an occurrence rate of $12.8^{+10.4}_{-7.2}$%. These relatively high estimates and uncertainties are reflective of the ranges involved and the higher frequency of planets with small masses and at small separations. The metaanalysis of Bowler (2016), which considered only companions on $a \geqslant 30$ au orbits and found a relatively low occurrence rate of wide-orbit planets orbiting BA stars ($\sim$3%), is also indicative of the bias of higher occurrence rates at small separations.

Considering planets with orbital semimajor axes of a = 60–80 au and masses of M = 5–15 $M_{\rm Jup}$, we find an occurrence rate of $3.4^{+5.4}_{-2.5}$% and a 95%-CL upper limit of $<$13.9%. In comparison, for M = 5–35 $M_{\rm Jup}$ companions at separations of a = 30–40 au (i.e., those at shorter orbital periods and including larger masses), we measure an occurrence rate of $\sim$10% and establish a 95%-CL upper limit of $\lesssim$45%. This illustrates the power of establishing sensitivity at smaller separations to dramatically increase the yield of direct imaging planet surveys. These results are also consistent with the majority of directly imaged planetary-mass companions at a $\lesssim$ 100 au forming via core accretion (e.g., Kratter et al. 2010; Wagner et al. 2019). In contrast, giant planets formed via gravitational instability should be more common at larger radii and around less-massive stars, as instabilities are more likely in the cold outer disk regions (e.g., Boss 1997).

Finally, our results offer a complementary sample to past studies that were largely focused on lower-mass stellar hosts in the solar neighborhood, and also to other ongoing surveys of both higher- and lower-mass stars in Sco OB2. Taken in combination with GPIES (Nielsen et al. 2019) and SHINE (Vigan et al. 2021), the BEASTS survey of B-type stars (Janson et al. 2021), and YSES survey (Bohn et al. 2020, 2021) of solar-type stars (both also focused on Sco OB2), these surveys provide a rich and comprehensive view of wide-orbit giant plants around nearby young stars. Together, they inform our understanding of exoplanet demographics, and perhaps of equal importance, enable the yield of future exoplanet imaging surveys to be enhanced by targeting stars around which detectable planets are more likely to exist.

5. Summary and Conclusions

We conducted a uniform blind survey for substellar companoions around 88 A-type stars in the Scorpius–Centaurus OB association with the VLT/SPHERE extreme-AO system. We detected three substellar companions—one of which, HIP 75056Ab, marks a new discovery. We computed the sensitivity to companions across a two-dimensional grid of separations and position angles with forward modeling of injected (simulated) planetary signals in the data, and utilized these results to explore the consistency with underlying planet populations through Monte Carlo simulations.

We find that giant planets on wide orbits (like HR 8799b and HIP 65426b) with masses of 5–15 $M_{\rm Jup}$ and semimajor axes of 60–80 au have an occurrence rate of $3.4^{+5.4}_{-2.5}$% and a 95%-CL upper limit of $\leqslant$13.9%. For companions between M = 5–35 $M_{\rm Jup}$, we measure frequencies between 10% and 2% for separations of 30–100 au, and 95% confidence-level upper limits of $\lesssim$45%–8% for planets on 30–100 au orbits, and $\lesssim$5% between 200 and 500 au. In line with other recent studies (e.g., Nielsen et al. 2019; Wagner et al. 2019; Vigan et al. 2021), we confirm the trend of increasing occurrence rates as a function of smaller separations. When compared to other studies of less-massive stars (e.g., Chauvin et al. 2003; Biller et al. 2007; Kasper et al. 2007; Stone et al. 2018; Nielsen et al. 2019; Vigan et al. 2021), we confirm a trend of more massive stars having a higher frequency of wide-orbit giant planets. This is consistent with exoplanet population trends among inner planetary

systems (e.g., Ghezzi et al. 2018; Mulders et al. 2021) and also with core accretion being the dominant formation mechanism among this population (e.g., Kratter et al. 2010; Wagner et al. 2019). Consequently, further progress to enable sensitivity to high-contrast ratios at small separations and a dedicated focus on young A-type stars should significantly raise the yield of exoplanet imaging surveys.

This work is based on observations performed with ESO's Very Large Telescope and SPHERE instrument under program IDs 095.C-0298, 095.C-0389, 096.C-0241, 296.C-5036, 097.C-0545, 097.C-0060, 097.C-0826, 097.C-0865, 097.C-0949, 097.C-1019, 099.C-0247, 099.C-0300, 099.C-0402, 0101.C-0513, 0103.C-0628, 198.C-0209, and 1100.C-0481. The results reported herein benefited from collaborations and/or information exchange within NASA's Nexus for Exoplanet System Science (NExSS) research coordination network sponsored by NASA's Science Mission Directorate. K.W. acknowledges support from NASA through the NASA Hubble Fellowship grant HST-HF2-51472.001-A awarded by the Space Telescope Science Institute, which is operated by the Association of Universities for Research in Astronomy, Incorporated, under NASA contract NAS5-26555.

Appendix
Target List

The targets of our survey are described below in Table A1.

Table A1
Targets—Sco-Cen A-type Stars

Target #	R.A. (J2000)	Decl. (J2000)	HIP #	K_s	SpT	Sub group	Date Obs. (YYYY-MM-DD)	Exp. Time (min)	Field Rot. (°)	Filter	DIT (sec)	Survey ID
1	10 19 05.1	−64 40 35	50520	6.23	A1V	LCC	2015-04-26	42.1	19.1	K12	8.00	S11
2	10 57 03.0	−68 40 02	53524	6.76	A8III	LCC	2019-04-13	101	33.8	K12	96.0	SA1_2
3	11 05 45.7	−47 26 32	54231	6.75	A0V	LCC	2015-02-06	68.3	39.2	*H*23	64.0	SA2
4	11 17 58.1	−64 02 33	55188	7.43	A2V	LCC	2016-05-20	25.6	9.77	K12	16.0	S41
5	11 27 29.4	−39 52 35	55899	7.07	A0V	LCC	2018-02-26	76.8	61.0	K12	96.0	SA3
6	11 33 05.6	−54 19 29	56354	5.78	A9V	LCC	2015-04-10	23.5	12.5	K12	8.00	S6
							2016-01-21	23.5	7.65	*H*23	8.00	S6_3
							2016-01-23	23.5	7.39	K12	8.00	S6_2
7	11 41 00.2	−54 32 56	56993	7.38	A0V	LCC	2016-06-05	22.4	12.1	K12	16.0	S44
							2019-04-09	27.9	15.2	K12	8.00	S44_2
8	11 51 13.1	−43 55 59	57809	6.61	A0V	LCC	2017-05-15	32.0	22.7	K12	16.0	S47
9	11 59 23.7	−57 10 05	58465	6.32	A2V	LCC	2016-03-30	64.0	27.9	*H*23	64.0	SA5
10	12 09 38.8	−58 20 59	59282	7.00	A3V	LCC	2017-05-04	68.3	34.8	K12	64.0	SA6
11	12 11 05.9	−56 24 05	59397	7.01	A2V	LCC	2017-06-01	31.5	14.5	K12	16.0	S51
12	12 11 14.8	−52 13 03	59413	7.46	A6V	LCC	2015-04-10	17.9	13.1	K12	8.00	S23
							2015-06-16	25.6	13.5	K12	16.0	S23_2
							2019-05-29	29.3	16.4	K12	8.00	S23_3
13	12 12 10.3	−63 27 15	59502	6.80	A2V	LCC	2018-03-24	32.0	12.3	K12	16.0	S63
							2019-05-26	29.9	12.3	K12	8.00	S63_2
14	12 17 06.3	−65 41 35	59898	5.99	A0V	LCC	2016-04-06	67.2	23.9	*H*23	64.0	SA7
15	12 24 51.9	−72 36 14	60561	6.59	A0V	LCC	2017-06-13	57.6	24.4	K12	96.0	SA8
16	12 28 19.3	−64 20 28	60851	5.98	A0Vn	LCC	2017-05-15	32.0	12.1	K12	16.0	S48
							2019-04-26	27.5	12.1	K12	8.00	S48_2
							2019-05-29	27.7	12.3	K12	8.00	S48_3
17	12 33 19.9	−54 58 52	61265	7.44	A2V	LCC	2016-04-23	19.2	10.9	K12	16.0	S35
							2019-04-09	29.1	15.1	K12	8.00	S35_2
18	12 38 07.3	−55 55 52	61639	6.94	A1/A2V	LCC	2017-06-01	31.5	14.9	K12	16.0	S52
19	12 39 46.2	−49 11 56	61782	7.56	A0V	LCC	2015-04-04	19.9	14.6	K12	8.00	S1
							2015-04-13	58.4	34.4	*H*23	16.0	S1_2*
20	12 57 26.2	−67 57 39	63236	6.66	A2IV/V	LCC	2017-06-15	51.2	33.9	K12	96.0	SA10
21	13 05 02.0	−64 26 30	63839	6.66	A0V	LCC	2016-04-17	83.2	30.5	*H*23	64.0	SA11
22	13 10 58.4	−52 34 01	64320	6.22	Ap	LCC	2015-04-09	21.6	12.8	K12	8.00	S4
							2017-06-22	31.2	16.3	K12	16.0	S4_2
23	13 18 24.9	−45 45 53	64925	6.88	A0V	LCC	2016-05-20	25.6	14.3	K12	16.0	S42
24	13 18 34.9	−51 17 09	64933	6.29	A0V	LCC	2015-05-01	18.8	13.6	K12	8.00	S15
							2019-05-26	29.9	17.1	K12	8.00	S15_2
25	13 20 26.8	−49 13 25	65089	7.37	A7/A8V	LCC	2017-07-01	31.7	18.4	K12	16.0	S55
							2018-04-08	27.7	16.0	K12	16.0	S55_2
26	13 21 57.1	−51 16 56	65219	6.52	A3/A4	LCC	2015-07-10	25.6	13.0	K12	16.0	S27
							2019-05-31	29.6	17.5	K12	8.00	S27_2
27	13 24 08.6	−53 47 35	65394	7.25	A1Vn	LCC	2018-04-10	76.8	35.5	K12	96.0	SA12
28	13 24 36.1	−51 30 16	65426	6.78	A2V	LCC	2017-02-09	59.7	49.1	K12	64.0	SA13
29	13 29 36.2	−47 52 33	65822	6.68	A1V	LCC	2015-06-11	24.5	15.1	K12	16.0	S20
30	13 32 39.2	−44 27 01	66068	7.04	A1/A2V	LCC	2017-05-07	25.6	17.5	K12	64.0	SA14
31	13 38 42.9	−44 30 59	66566	7.36	A1V	LCC	2015-05-15	50.1	33.6	*H*23	64.0	SA15
32	13 40 37.7	−44 19 49	66722	6.32	A0V	UCL	2018-02-22	32.0	21.9	K12	16.0	S60
							2019-05-25	20.9	22.7	K12	8.00	S60_2

Table A1
(Continued)

Target #	R.A. (J2000)	Decl. (J2000)	HIP #	K_s	SpT	Sub group	Date Obs. (YYYY-MM-DD)	Exp. Time (min)	Field Rot. (°)	Filter	DIT (sec)	Survey ID
							2019-06-27	28.5	22.8	K12	8.00	S60_3
							2019-06-30	29.6	21.7	K12	16.0	S60_4
33	13 44 16.0	−51 00 45	67036	6.69	A0p	LCC	2015-07-17	25.6	13.3	K12	16.0	S30
34	13 56 20.0	−54 07 57	68080	6.28	A1V	UCL	2016-06-05	32.3	17.0	*H*23	16.0	SA17
35	14 01 45.7	−39 26 19	68532	7.03	A3IV/V	UCL	2015-04-09	23.3	23.5	K12	8.00	S5
							2019-05-09	29.6	27.9	K12	8.00	S5_2
							2019-05-29	29.5	29.9	K12	8.00	S5_3
36	14 04 42.1	−50 04 17	68781	7.38	A2V	UCL	2016-03-30	42.7	27.8	*H*23	64.0	SA18
37	14 06 08.2	−44 41 21	68867	7.17	A0V	UCL	2017-06-24	32.0	22.0	K12	16.0	S53
38	14 06 58.2	−47 35 21	68958	6.72	Ap...	UCL	2015-04-15	23.3	15.7	K12	8.00	S7
							2018-03-15	27.7	16.8	K12	16.0	S7_2
39	14 24 37.0	−47 10 40	70441	7.31	A1V	UCL	2016-07-23	42.7	25.2	*H*23	32.0	SA19
40	14 27 33.6	−46 12 49	70697	7.17	A0V	UCL	2015-05-11	72.5	51.6	*H*23	64.0	SA20
41	14 28 51.9	−47 59 32	70809	6.54	Ap...	UCL	2017-07-24	38.1	33.1	K12	16.0	S56
42	14 29 58.4	−56 07 52	70904	6.39	A6V	UCL	2015-06-09	25.6	12.0	K12	16.0	S18
							2017-05-15	32.0	14.7	K12	16.0	S18_2
43	14 30 10.0	−43 51 50	70918	6.35	A0/A1V	UCL	2017-06-24	30.9	22.9	K12	16.0	S54
44	14 32 57.1	−42 24 20	71140	7.13	A7/A8IV	UCL	2015-04-29	42.7	34.8	K12	8.00	S12
							2019-06-29	29.9	25.3	K12	8.00	S12_2
45	14 34 33.4	−46 18 17	71271	7.57	A0V	UCL	2017-05-29	65.1	48.1	*H*	32.0	SA21
46	14 40 19.3	−45 47 38	71727	6.89	A0p	UCL	2015-04-06	21.1	24.0	K12	8.00	S3
							2019-06-27	29.6	21.5	K12	8.00	S3_2
47	14 45 20.6	−36 08 52	72140	7.09	A1IV/V	UCL	2016-04-06	25.6	30.7	K12	16.0	S34
							2019-05-26	29.9	35.5	K12	8.00	S34_2
48	14 45 57.6	−44 52 03	72192	6.71	A0V	UCL	2015-06-11	25.6	17.3	K12	16.0	S21
49	14 50 58.7	−42 49 21	72627	6.53	A2V	UCL	2016-04-23	24.0	19.6	K12	16.0	S36
							2019-05-26	29.9	23.4	K12	8.00	S36_2
50	14 54 25.3	−34 08 34	72940	6.85	A1V	UCL	2015-06-12	25.6	36.8	K12	16.0	S22
							2016-03-06	33.6	38.5	K12	32.0	S22_2
							2016-03-17	29.9	36.6	K12	32.0	S22_3
							2016-05-07	29.9	39.6	K12	32.0	S22_4
							2017-05-31	27.7	23.1	*Y*23	16.0	S22_5
							2017-07-22	27.7	3.89	*H*23	16.0	S22_6
							2017-07-23	26.1	5.59	K12	32.0	S22_7
							2017-07-23	24.5	3.78	*Ks*	32.0	S22_8
							2017-07-24	27.2	10.7	*J*23	16.0	S22_9
							2017-07-28	26.9	10.2	*H*23	16.0	S22_10
							2018-03-14	27.5	38.9	*H*23	16.0	S22_11
							2018-07-14	34.1	38.0	K12	16.0	S22_12
51	14 54 54.5	−36 25 49	72984	7.05	A0/A1V	UCL	2018-03-16	40.0	52.4	K12	16.0	S61
52	14 56 54.5	−35 41 44	73145	7.54	A2IV	UCL	2015-05-14	67.2	72.5	*H*23	64.0	SA22
53	14 59 54.6	−46 14 53	73393	7.21	A0V	UCL	2015-07-17	25.6	14.2	K12	16.0	S29
							2019-05-10	29.9	21.2	K12	8.00	S29_2
54	15 06 33.2	−30 55 07	73937	6.05	Ap	UCL	2018-03-16	32.0	21.9	K12	16.0	S62
55	15 17 10.7	−34 34 37	74797	7.55	A2IV	UCL	2015-04-29	23.5	33.9	K12	8.00	S13
							2019-06-27	22.3	30.3	K12	8.00	S13_2
56	15 19 22.3	−34 01 57	74985	7.53	A0V	UCL	2017-05-15	31.2	45.1	K12	16.0	S49
57	15 20 13.4	−34 55 32	75056	7.31	A2V	UCL	2015-06-19	21.3	13.8	K12	16.0	S25
							2019-06-29	28.5	41.6	K12	8.00	S25_2
58	15 20 31.4	−28 17 14	75077	6.97	A1V	UCL	2016-04-03	16.4	25.7	*H*23	4.00	SA23
59	15 21 30.1	−38 13 07	75151	6.65	A+...	UCL	2015-07-18	25.6	18.7	K12	16.0	S31
60	15 25 30.2	−36 11 58	75509	7.40	A2V	UCL	2018-04-10	76.8	75.6	K12	96.0	SA25
61	15 30 48.4	−45 25 28	75957	7.24	A0V	UCL	2015-07-12	41.9	27.8	K12	16.0	S28
							2019-05-01	29.9	21.7	K12	8.00	S28_2
62	15 46 51.6	−36 56 13	77295	7.64	A2IV/V	UCL	2017-05-15	32.0	32.2	K12	16.0	S50
63	15 48 52.1	−29 29 00	77457	7.33	A7IV	US	2015-06-09	25.6	12.0	K12	16.0	S18
							2017-05-15	32.0	14.7	K12	16.0	S18_2
64	15 56 47.9	−23 11 03	78099	7.35	A0V	US	2015-05-09	27.7	8.19	*H*23	64.0	SA26
65	15 57 59.3	−31 43 44	78196	7.08	A0V	US	2015-06-03	57.6	84.6	*H*23	64.0	SA27
66	16 01 26.6	−25 11 55	78494	7.11	A2m...	US	2015-05-18	22.1	2.34	K12	8.00	S16
67	16 01 58.9	−37 32 04	78533	6.99	Ap	UCL	2016-07-14	24.3	24.8	K12	16.0	S45
							2019-05-12	36.3	32.1	K12	8.00	S45_2
68	16 02 04.8	−36 44 38	78541	6.99	A0V	UCL	2015-05-19	23.5	12.5	K12	8.00	S17

Table A1
(Continued)

Target #	R.A. (J2000)	Decl. (J2000)	HIP #	K_s	SpT	Sub group	Date Obs. (YYYY-MM-DD)	Exp. Time (min)	Field Rot. (°)	Filter	DIT (sec)	Survey ID
69	16 04 44.5	−39 26 05	78756	7.16	Ap	UCL	2016-04-23	25.1	18.4	K12	16.0	S37
							2016-08-07	22.7	20.9	K12	16.0	S37_2
							2017-05-29	31.5	28.3	K12	16.0	S37_3
70	16 05 43.4	−21 50 20	78847	7.32	A0V	US	2015-06-17	25.6	2.59	K12	16.0	S24
71	16 05 46.3	−39 50 36	78853	7.50	A5V	UCL	2016-04-23	19.5	23.9	K12	16.0	S38
72	16 07 29.9	−23 57 02	78996	7.46	A9V	US	2015-06-19	25.6	0.558	K12	16.0	S26
73	16 11 52.7	−22 32 42	79366	7.47	A3V	US	2017-07-28	29.9	2.65	K12	16.0	S59
74	16 18 05.5	−31 39 06	79860	7.88	A0V	US	2015-07-31	18.7	37.6	K12	16.0	S33
75	16 18 16.2	−28 02 30	79878	7.06	A0V	US	2016-07-02	40.4	17.9	*H*23	8.00	SA28
76	16 20 04.0	−20 02 42	80019	7.08	A0V	US	2015-04-21	23.5	355.	K12	8.00	S9
							2019-05-31	29.9	36.2	K12	8.00	S9_2
77	16 20 28.1	−21 30 32	80059	7.44	A7III/IV	US	2017-07-25	32.0	4.21	K12	16.0	S57
78	16 23 56.7	−33 11 58	80324	7.33	A0V	US	2018-06-18	59.2	53.1	*H*23	96.0	SA29
79	16 25 35.1	−23 24 19	80474	5.76	A	US	2017-07-27	32.0	0.252	K12	16.0	S58
80	16 27 14.6	−39 49 22	80591	7.82	A5V	UCL	2015-04-05	20.4	30.0	K12	8.00	S2
							2017-05-29	26.4	28.8	K12	16.0	S2_2
81	16 29 54.6	−24 58 46	80799	7.46	A2V	US	2016-08-07	25.3	2.09	K12	16.0	S46
82	16 31 11.7	−38 22 59	80897	7.78	A0V	UCL	2015-07-19	23.5	19.5	K12	16.0	S32
							2017-05-28	32.0	29.7	K12	16.0	S32_2
83	16 34 10.5	−38 23 25	81136	5.21	A7/A8	UCL	2016-04-23	26.3	28.4	K12	8.00	S39
							2019-05-01	29.9	32.3	K12	8.00	S39_2
84	16 41 52.0	−40 27 58	81751	8.29	A9V	UCL	2015-04-29	23.5	22.0	K12	8.00	S14
							2017-06-22	31.7	27.2	K12	16.0	S14_2
85	16 44 21.1	−44 22 43	81949	7.32	A3V	UCL	2016-04-23	25.1	15.7	K12	16.0	S40
86	16 52 31.9	−42 59 30	82560	6.58	A0V	UCL	2016-05-20	25.6	17.5	K12	16.0	S43
							2019-04-28	29.9	24.1	K12	8.00	S43_2
87	17 03 22.2	−40 05 16	83457	6.49	A9V	UCL	2015-04-15	23.2	19.4	K12	8.00	S8
							2016-04-23	21.3	11.4	K12	16.0	S8_2
88	17 06 20.2	−37 13 39	83693	5.69	A2IV	UCL	2015-04-23	21.9	28.0	K12	8.00	S10
							2016-08-11	25.5	25.8	K12	8.00	S10_2
							2017-05-29	30.1	32.1	K12	16.0	S10_3

Note. Survey IDs were assigned in numerical order as observations were completed, except for those obtained from the archive (those beginning with "SA"), which were assigned in order of increasing R.A. (R.A.). The other abbreviations in the column headers are Dec. (decl.), SpT (Spectral Type), and DIT (Detector Integration Time).

ORCID iDs

Kevin Wagner https://orcid.org/0000-0002-4309-6343
Dániel Apai https://orcid.org/0000-0003-3714-5855
Markus Kasper https://orcid.org/0000-0002-8425-6606
Massimo Robberto https://orcid.org/0000-0002-9573-3199

References

Apai, D., Janson, M., Moro-Martín, A., et al. 2008, ApJ, 672, 1196
Apai, D., Kasper, M., Skemer, A., et al. 2016, ApJ, 820, 40
Bailey, V., Meshkat, T., Reiter, M., et al. 2014, ApJL, 780, L4
Baraffe, I., Chabrier, G., Allard, F., et al. 1998, A&A, 337, 403
Baraffe, I., Chabrier, G., Barman, T. S., et al. 2003, A&A, 402, 701
Baraffe, I., Homeier, D., Allard, F., et al. 2015, A&A, 577, A42
Beuzit, J.-L., Vigan, A., Mouillet, D., et al. 2019, A&A, 631, A155
Biller, B. A., Close, L. M., Masciadri, E., et al. 2007, ApJS, 173, 143
Bohn, A. J., Ginski, C., Kenworthy, M. A., et al. 2021, A&A, 648, A73
Bohn, A. J., Kenworthy, M. A., Ginski, C., et al. 2020, ApJL, 898, L16
Boss, A. P. 1997, Sci, 276, 1836
Bowler, B. P. 2016, PASP, 128, 102001
Bowler, B. P., Blunt, S. C., & Nielsen, E. L. 2020, AJ, 159, 63
Brandt, T. D., McElwain, M. W., Turner, E. L., et al. 2014, ApJ, 794, 159
Chauvin, G., Desidera, S., Lagrange, A.-M., et al. 2017, A&A, 605, L9
Chauvin, G., Thomson, M., Dumas, C., et al. 2003, A&A, 404, 157
Claudi, R. U., Turatto, M., Gratton, R. G., et al. 2008, Proc. SPIE, 7014, 70143E
De Rosa, R. J., Rameau, J., Patience, J., et al. 2016, ApJ, 824, 121
de Zeeuw, P. T., Hoogerwerf, R., de Bruijne, J. H. J., et al. 1999, AJ, 117, 354
Dong, R., Zhu, Z., Fung, J., et al. 2016, ApJL, 816, L12
Emsenhuber, A., Mordasini, C., Burn, R., et al. 2021, A&A, 656, A69
Fernandes, R. B., Mulders, G. D., Pascucci, I., et al. 2019, ApJ, 874, 81
Forgan, D. H., Hall, C., Meru, F., et al. 2018, MNRAS, 474, 5036
Fortney, J. J., Marley, M. S., Saumon, D., et al. 2008, ApJ, 683, 1104
Fulton, B. J., Rosenthal, L. J., Hirsch, L. A., et al. 2021, ApJS, 255, 14
Ghezzi, L., Montet, B. T., & Johnson, J. A. 2018, ApJ, 860, 109
Gaia Collaboration, Brown, A. G. A., Vallenari, A., et al. 2018, A&A, 616, A1
Haffert, S. Y., Bohn, A. J., de Boer, J., et al. 2019, NatAs, 3, 749
Holman, M. J., & Wiegert, P. A. 1999, AJ, 117, 621
Janson, M., Squicciarini, V., Delorme, P., et al. 2021, A&A, 646, A164
Jovanovic, N., Martinache, F., Guyon, O., et al. 2015, PASP, 127, 890
Kasper, M., Apai, D., Janson, M., et al. 2007, A&A, 472, 321
Kasper, M., Apai, D., Wagner, K., et al. 2015, ApJL, 812, L33
Keppler, M., Benisty, M., Müller, A., et al. 2018, A&A, 617, A44
Kouwenhoven, M. B. N., Brown, A. G. A., Portegies Zwart, S. F., et al. 2007, A&A, 474, 77
Kouwenhoven, M. B. N., Brown, A. G. A., Zinnecker, H., et al. 2005, A&A, 430, 137
Kratter, K. M., Murray-Clay, R. A., & Youdin, A. N. 2010, ApJ, 710, 1375
Lagrange, A.-M., Bonnefoy, M., Chauvin, G., et al. 2010, Sci, 329, 57
Lagrange, A.-M., Keppler, M., Beust, H., et al. 2017, A&A, 608, L9
Lannier, J., Delorme, P., Lagrange, A. M., et al. 2016, A&A, 596, A83
Macintosh, B., Graham, J. R., Barman, T., et al. 2015, Sci, 350, 64
Macintosh, B., Graham, J. R., Ingraham, P., et al. 2014, PNAS, 111, 12661
Maire, A.-L., Langlois, M., Dohlen, K., et al. 2016, Proc. SPIE, 9908, 990834
Males, J. R., Close, L. M., Miller, K., et al. 2018, Proc. SPIE, 10703, 1070309
Marleau, G.-D., Mordasini, C., & Kuiper, R. 2019, ApJ, 881, 144

Marley, M. S., Fortney, J. J., Hubickyj, O., et al. 2007, ApJ, 655, 541
Marois, C., Lafrenière, D., Doyon, R., et al. 2006, ApJ, 641, 556
Marois, C., Macintosh, B., Barman, T., et al. 2008, Sci, 322, 1348
Marois, C., Zuckerman, B., Konopacky, Q. M., et al. 2010, Natur, 468, 1080
Mawet, D., Milli, J., Wahhaj, Z., et al. 2014, ApJ, 792, 97
Mordasini, C., Alibert, Y., & Benz, W. 2009, A&A, 501, 1139
Mordasini, C., Alibert, Y., Klahr, H., et al. 2012, A&A, 547, A111
Mulders, G. D., Pascucci, I., Ciesla, F. J., et al. 2021, ApJ, 920, 66
Nealon, R., Cuello, N., Gonzalez, J.-F., et al. 2020, MNRAS, 499, 3857
Nielsen, E. L., De Rosa, R. J., Macintosh, B., et al. 2019, AJ, 158, 13
Nielsen, E. L., Liu, M. C., Wahhaj, Z., et al. 2013, ApJ, 776, 4
Nielsen, E. L., Rosa, R. J. D., Rameau, J., et al. 2017, AJ, 154, 218
Pascucci, I., Testi, L., Herczeg, G. J., et al. 2016, ApJ, 831, 125
Pecaut, M. J., & Mamajek, E. E. 2016, MNRAS, 461, 794
Pollack, J. B., Hubickyj, O., Bodenheimer, P., et al. 1996, Icar, 124, 62
Rameau, J., Chauvin, G., Lagrange, A.-M., et al. 2013, ApJL, 779, L26
Soummer, R., Pueyo, L., & Larkin, J. 2012, ApJL, 755, L28
Stone, J. M., Skemer, A. J., Hinz, P. M., et al. 2018, AJ, 156, 286
Su, K. Y. L., MacGregor, M. A., Booth, M., et al. 2017, AJ, 154, 225
Vigan, A., Fontanive, C., Meyer, M., et al. 2021, A&A, 651, A72
Vigan, A., Moutou, C., Langlois, M., et al. 2010, MNRAS, 407, 71
Wagner, K., Apai, D., Kasper, M., et al. 2015, ApJL, 813, L2
Wagner, K., Apai, D., Kasper, M., et al. 2016, Sci, 353, 673
Wagner, K., Apai, D., Kasper, M., et al. 2020, ApJL, 902, L6
Wagner, K., Apai, D., & Kratter, K. M. 2019, ApJ, 877, 46
Wagner, K., Dong, R., Sheehan, P., et al. 2018, ApJ, 854, 130
Wagner, K., Follete, K. B., Close, L. M., et al. 2018, ApJL, 863, L8
Zapata, L. A., Ho, P. T. P., & Rodríguez, L. F. 2018, MNRAS, 476, 5382